Cell Reports, Volume *14*

Supplemental Information

The Innate Immune Receptor NLRX1 Functions as a Tumor Suppressor by Reducing Colon Tumorigenesis and Key Tumor-Promoting Signals

A. Alicia Koblansky, Agnieszka D. Truax, Rongrong Liu, Stephanie A. Montgomery, Shengli Ding, Justin E. Wilson, W. June Brickey, Marcus Mühlbauer, Rita-Marie T. McFadden, Peizhen Hu, Zengshan Li, Christian Jobin, Pauline Kay Lund, and Jenny P.-Y. Ting

Supplemental Figures

A

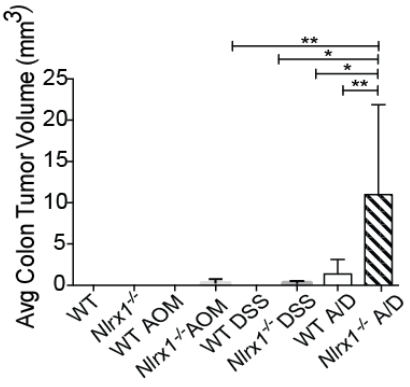

B

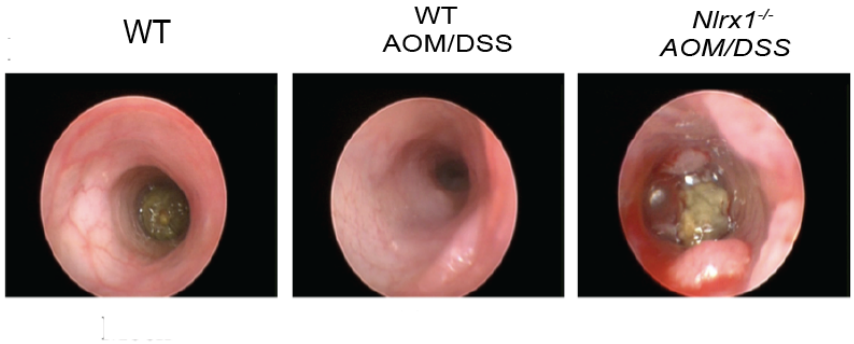

Figure S1

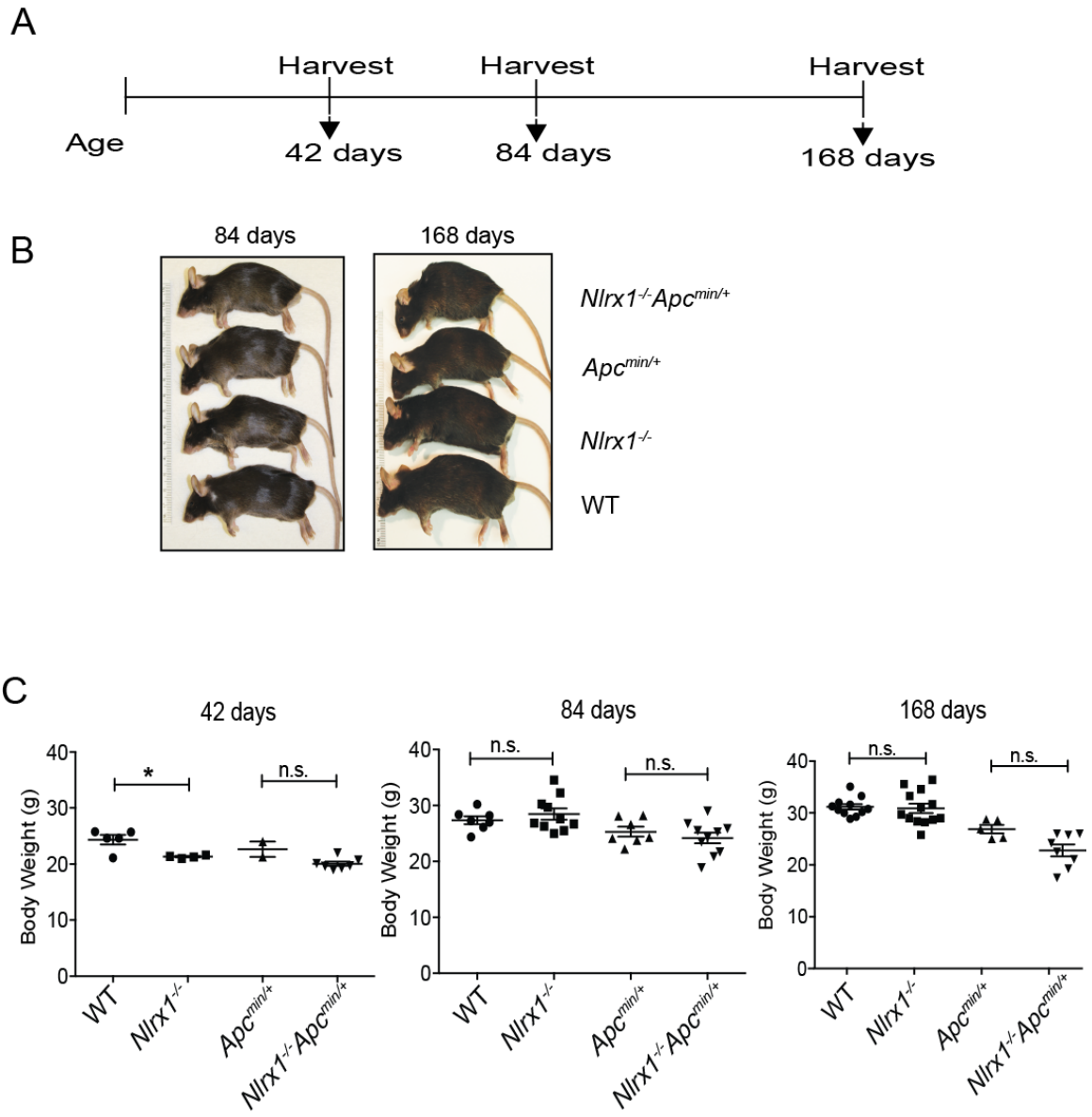
A
Harvest
Harvest
Harvest
Age
42 days
84 days
168 days
B
84 days
168 days
Nlrx1-/-Apcmin/+
Apcmin/+
Nlrx1-/-
WT
C
42 days
84 days
168 days
Body Weight (g)
0
10
20
30
40
*
n.s.
WT
Nlrx1-/-
Apcmin/+
Nlrx1-/-Apcmin/+

Figure S2

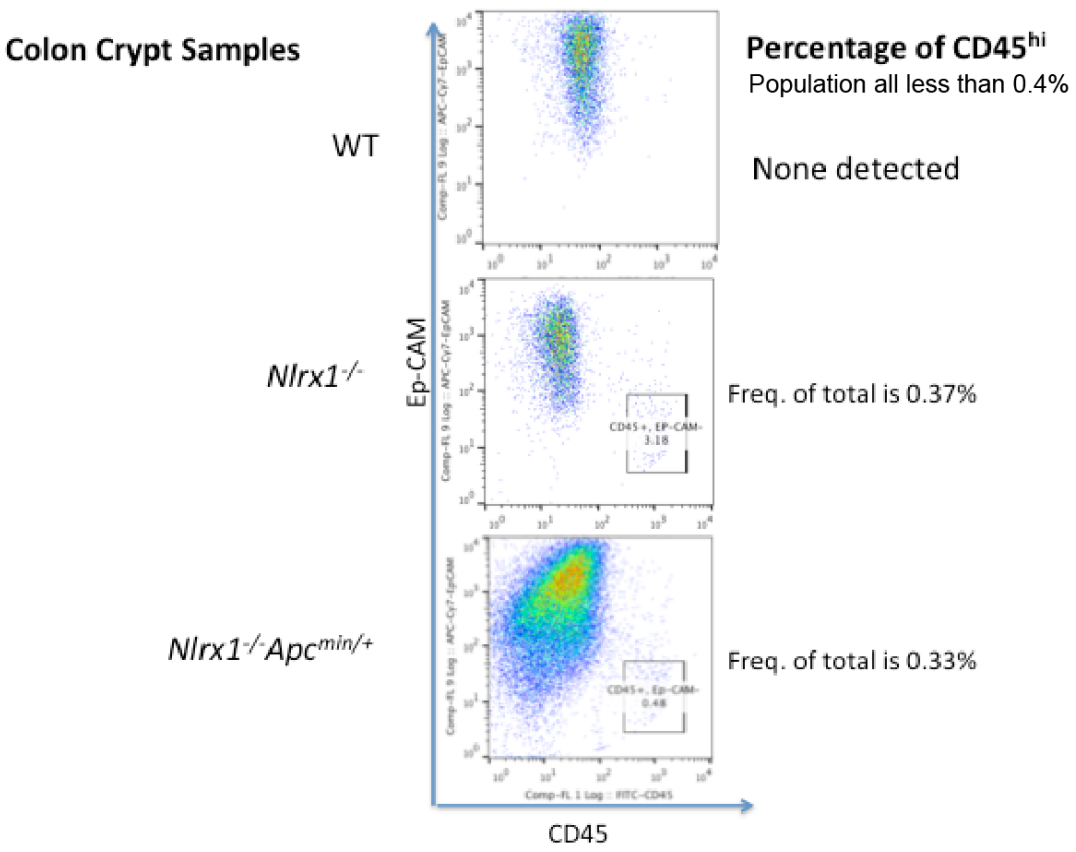
Colon Crypt Samples
Percentage of CD45hi
Population all less than 0.4%
WT
None detected
Nlrx1-/-
Freq. of total is 0.37%
Nlrx1-/-Apcmin/+
Freq. of total is 0.33%
Ep-CAM
CD45
CD45+, EP-CAM- 3.18
CD45+, Ep-CAM- 0.48

Figure S3

SUPPLEMENTAL FIGURE LEGENDS

Figure S1 (related to Figure 1): After AOM/DSS treatment, *Nlrx1*$^{-/-}$ mice have increased tumor burden compared to WT animals. (A) *Nlrx1*$^{-/-}$ animals have significantly increased tumor volume compared to WT animals during AOM/DSS-induced CAC. Tumor volumes were determined as the average sum of the volumes [V = (width^2 x length)/2] of all colon tumors per mouse**.** (B) *Nlrx1*$^{-/-}$ and WT mice challenged with AOM and 3% DSS showed more polyps as assessed by an endoscopic examination. Endoscopy of untreated WT mice and AOM/DSS-treated WT and *Nlrx1*$^{-/-}$ mice forty-eight days after the first DSS treatment. Images are representative of two mice for each condition.

Figure S2 (related to Figure 3): *Nlrx1*$^{-/-}$*Apc*$^{min/+}$ mice display a more severe phenotype, but no significant difference in weight compared to controls. (A) Schematic of harvest times of indicated animals at 168, 84, and 42 days of age to elucidate potential causes of early mortality in the *Apc*$^{min/+}$ model. (B) Images of WT*, Nlrx1*$^{-/-}$*, Apc*$^{min/+}$ and *Nlrx1*$^{-/-}$*Apc*$^{min/+}$ mice at 84 and 168 days of age. (C) Comparison of body weights from *Nlrx1*$^{-/-}$*Apc*$^{Min/+}$, *APC*$^{min/+}$, *Nlrx1*$^{-/-}$ and WT mice at 42, 84 and 168 days. Each data point represents one animal. n.s., non-significant, *p<0.05, **p<0.01 and ****p<0.0001.

Figure S3 (Related to Figure 5): FACS analysis of colon crypts. Colon crypt cells were collected from four different strains of mice: WT, *Nlrx1*$^{-/-}$, *APC*$^{min/+,}$ and

Nlrx1$^{-/-}$*Apc*$^{min/+}$. Cells were stained with both CD45-FITC and EpCAM-APC in FACS staining buffer. FACS analysis revealed that the isolated colon crypt cells were EpCAM^{Hi} and CD45^{Lo}. The frequency of CD45^{+} cells in the colon crypt cell populations were determine to be < 0.4%.

SUPPLEMENTAL EXPERIMENTAL PROCEDURES:

Animals: All experiments were performed under specific-pathogen-free (SPF) conditions. Sentinel mice were routinely monitored for bacterial, viral, ecto, and endoparasitic pathogens so to confirm SPF condition. For littermates, heterozygous mice were breed and maintained for experimental work.

Induction of experimental chronic colitis and colitis-associated colon cancer (CAC): To induce chronic colitis, littermates were given three cycles of 3% DSS for 5 days followed by 14 days of regular drinking water (Neufert et al., 2007). To Induce CAC, animals were given a single i.p. injection of the mutagen azoxymethane (AOM, 10 mg/kg body weight) (Sigma-Aldrich) in combination with three cycles of 3% DSS in drinking water for 5 days followed by regular drinking water for 14 days. Animals were euthanized at the end of the study on day 55 or when moribund with weight loss greater than 20% as stated in our IACUC-approved protocol. Animals were monitored for weight loss daily during DSS treatment and once every two days during regular water administration to measure disease progression. Furthermore, clinical score assessments were blindly performed after each round of DSS at days 7, 26, and 45, which consisted assessments of body condition, stool consistency, rectal bleeding and presence of stool blood measured using Hemoccult Immunochemical Fecal Occult (Beckman Coulter) as previously described (Allen et al., 2010). Tumor volumes were determined as the average sum of the volumes [$V = (\text{width}^2 \times \text{length})/2$] of all colon tumors per mouse.

Radiation bone marrow chimeras: Radiation bone marrow chimeric mice were generated as previously described (Allen et al., 2010). Briefly, 10-12 week-old wild type ($CD45.1^+$) and *Nlrx1*$^{-/-}$ (CD45.2) mice were lethally irradiated (10 Gy) and i.v. injected with 10^7 bone marrow cells isolated from either wild type $CD45.1^+$ or *Nlrx1*$^{-/-}$ mice 24 hours post total body irradiation. Recipient mice were given 2 mg/ml neomycin in drinking water for 14 days and housed for an additional 56 days to allow for full bone marrow reconstitution before administration of AOM/DSS.

Molecular imaging of proteases: To quantify cathepsin B activity, an indirect imaging approach using a cathepsin B-catalyzable fluorescent target as described previously (Ding et al., 2014; Ding et al., 2012) was utilized. Specifically, the Near Infrared Fluorescence imaging probe ProSense 680 (PerkinElmer, Cat# NEV10003) emits a signal when activated by proteases with the highest specificity demonstrated by cathepsin B (Jaffer et al., 2008) and has been used for intestinal tumor detection (Zhang et al., 2008). The probe was administered to mice via retro-orbital injection. Animals were euthanized by an i.p. injection of Nembutal (100 mg/kg body weight) 24 hours later, and gastrointestinal tissues were harvested. Each part of colon was gently flushed with ice cold 1X PBS and imaged *ex vivo* by fluorescence reflectance imaging (FRI) (FMT 2500™ LX System, PerkinElmer). The light source energy level, exposure time and the distance from specimen to camera were kept constant across animals. During FRI imaging, the imaging system automatically adjusts

the scale to encompass the minimum-maximum of the signal for optimal visualization, with a higher scale reflecting a stronger signal.

Assessment of colon polyps: *In situ* mini-endoscopy was used to visualize *in vivo* tumor formation in mouse colons. Prior to endoscopy, animals were fasted overnight to minimize fecal obstruction. Endoscopy was performed by a trained gastroenterologist (M.M.) on animals under oxygen-regulated isoflurane (Minrad, Inc) sedation on day 48 of the AOM/DSS model using a Coloview system (Karl Storz Veterinary Endoscope) as previously described (Uronis et al., 2009). Colons were air inflated for real time visualization of 3-4 cm of colon from anal verge to the splenic flexure. The gastroenterologist was blinded to the genotype and experimental conditions. In addition, upon the completion of the AOM/DSS model, animals were euthanized and colons were removed, flushed with PBS and open longitudinally for visual polyp count.

Histopathology and immunohistochemistry: To visualize tissue pathology, isolated colons were flushed with PBS, prepared as Swiss rolls, fixed in 10% formalin and embedded in paraffin. Hematoxylin and eosin (H&E) staining was performed on 5-micron-thick sections, and hyperplasia and dysplasia were blindly evaluated by a Board-certified veterinary pathologist. Briefly, individual lesions were scored as described previously (Meira et al., 2008), and a total histology score for each specimen was completed by summing the individual lesion scores. Additional sections were stained for the tumorigenesis marker β-

catenin [E247] (Abcam), cleaved Caspase-3 (Abcam), and and Ki67 (Vector Laboratories). Measurements for percentage of cleaved Caspase-3^+ and Ki-67^+ cells were collected from 20 crypts that were sectioned longitudinal; half length of each colon crypt was measured from the basal layer. This was performed on three independent mice per strain.

RNA isolation and analysis: Inflammatory cytokine expression during colitis and CAC was assessed by washing colons with PBS and homogenizing the distal-most section for total RNA extraction using Trizol (Invitrogen). Following RNA isolation, total RNA was eluted with distilled water, and the RNA concentration was measured using a Nanodrop 2000 spectrophotometer. Subsequently iScript™ cDNA Synthesis Kit 170-8891 (Bio-Rad Laboratories, Inc.) was used to generate cDNA. Quantitative RT-PCR was performed on a ViiA™ 7 Real-Time PCR System. Quantitative PCR for mouse *Il1b* (Mm00434228_m1)*, Il6* (Mm00446190_m1) and *Tnfa* (Mm00443258_m1) was performed using TaqMan primer/probe sets and master mix (Applied Biosystems). To normalize the qPCR results, *Gapdh* (Mm99999915_g1) and *Actb* (Mm01324804_m1) were chosen as reference genes. All samples were loaded in triplicate. Relative mRNA expression levels were determined via the $2^{-\Delta\Delta CT}$ method or log-transformed.

Tissue homogenization and western blot analysis: Isolated colon tissue sections (1 cm) were homogenized using a Mini-Rottor (BioSpec). Tissues were

lysed in complete RIPA (Boston BioProducts) buffer for western blot analysis containing Complete Protease Inhibitor cocktail (Roche) and phosphatase inhibitor cocktail (phosSTOP, Roche). All protein lysates were quantified using a quantitative BCA protein Assay (Thermo Scientific). A total of 30 µg of protein was mixed in SDS loading dye containing 20 mg/ml DTT reducing agent, boiled for 5 min, separated by SDS-PAGE using 4-12% Bis-Tris gels (Novex) and wet transferred to nitrocellulose membrane (Roche). Nitrocellulose membranes were blocked for 1 hr with 10% non-fat milk and incubated overnight with primary antibodies, washed 5 times with TBS-T and incubated for 1-2 hrs at RT with the appropriate goat anti-rabbit or bovine anti-goat HRP conjugated secondary antibodies (Santa Cruz and Sigma Aldrich). Protein expression was determined using the following antibodies: phospho-IκBα (Cell Signaling), IκBα (Santa Cruz), phospho-p65 (Cell Signaling), p65 (Cell Signaling), phospho-ERK1/2 (Cell Signaling), ERK1/2 (Santa Cruz), phospho-JNK1/2 (Cell Signaling), JNK1/2 (Santa Cruz), phospho-STAT3 (Cell Signaling), STAT3 (Cell Signaling) and Actin (Santa Cruz).

Isolation of colon crypts: Following a previously described protocol (Fuller et al., 2013), colons were removed and flushed with cold PBS. Colons were cut into 2-3 cm pieces and transferred to 3mM EDTA/1.5mM DTT in PBS and place on ice for 30 minutes. After manual shaking for 30 seconds, the tissue is moved to fresh cold PBS with 3 mM EDTA and placed at 37°C for 10 minutes. Samples were shaken vigorously for 1 minute to separate the colon crypts from the

submucosa. The submucosa was discarded, the samples were spun at 300 x g for 5 minutes and the pellet was frozen for protein preparation.

Flow cytometric analysis of colon crypt cells. Colon crypt cells were collected and washed with PBS, re-suspended in FACS staining buffer (PBS supplemented with 5% fetal bovine serum) and counted. A total of 10^7 cells/mL were stained with both CD45-FITC (BD Bioscience) and EpCAM-APC (BD Bioscience) in FACS staining buffer. Flow cytometry was performed using an LSRII (BD Biosciences), and the resulting data was analyzed using FlowJo (TreeStar).

Colon tissue explants for the analysis of cytokine production: Colon cytokine secretion was assessed by flushing colons with PBS containing penicillin/streptomycin. The distal-most 1-cm^2 colon sections were cultured for 15 h in RPMI media containing penicillin/streptomycin. Supernatants from these cultures were removed, cleared of debris by centrifugation and assessed for mouse cytokines by ELISA (BD Biosciences).

Anti-IL-6R Antibody Treatment of Mice: IL-6 blockade was achieved using an intraperitoneal injection of 20 μg/mL of Tocilizumab (Genentech) every two weeks for 10 weeks. Animals of 6 weeks of age were monitored weekly for weight changed and body condition after initiation of antibody treatment.

Bioinformatics analysis of *NLRX1* expression in human CRC: Microarray studies containing data that focused on the expression of *NLRX1* in CRC were

obtained using the gene search function of the Oncomine® Platform (www.oncomine.org). The default parameters set by the platform were used: threshold fold change was greater or equal to 1.5X, *p* value was greater or equal to 0.0001 and the gene rank was in the top 10%. Data analysis was expressed as fold change of expression in CRC compared to normal tissues (Wang et al., 2014). Data from the five CRC datasets were designated by the first author and by the numbers of patient [CRC/normal controls]: Gaedcke [65/65] (Gaedcke et al., 2010), Skrzypczak [81/24] (Skrzypczak et al., 2010), TCGA colon cancer [215/22] (Cancer Genome Atlas, 2012), Kaiser [100/5] (Kaiser et al., 2007) and Graudens [18/12] (Graudens et al., 2006). Following an analysis of *NLRX1* expression, the results from these databases were sorted based on the *p* value, and the log-transformed median centered raw data were downloaded from the Oncomine® Platform. Graph Pad software was used to create the boxplots and dot figures.

Collection of clinical CRC specimens: Bio-specimens were collected from 40 patients newly diagnosed with colon or rectum adenocarcinoma as previously described (Liu et al., 2015). These patients underwent surgical resection during 2014 at the Xijing Hospital in Xi'an, China. None of the patients in this analysis received any prior treatment including chemotherapy and/or radiotherapy. All of the samples were collected and stored in agreement with the approved protocols of Xijing Hospital. The IRB was approved by the Institutional Research Ethics Committees in Xijing Hospital, Xi'an, China. Samples that were used for our

analyses were numbered and did not include any patient identifying information that is protected under the IRB agreement.

Cases were staged according to the American Joint Committee on Cancer staging system (AJCC) (Cancer Genome Atlas, 2012). Adjacent normal tissue specimens taken at a distance that is >2 cm from the actual tumor were used as controls. Histologic sections were obtained from top and bottom portions of each formalin-fixed and paraffin embedded (FFPE) specimen. Each tumor specimen weighed between 60 and 200 mg. Normal and cancerous sample were stained with H&E and examined by two board-certified pathologists (P.H. and Z.L.) to confirm the presence of CRC in the specimens. The pathologists confirmed that each tumor sample was histologically consistent with colon adenocarcinoma and that tumor cells were not present in the adjacent normal specimen (Cancer Genome Atlas, 2012).

RNA extraction from FFPE tissues and quantitative real-time PCR: RecoverAll™ Total Nucleic Acid Isolation Kit was used to isolate RNA from FFPE tissues according to the manufacturer's protocol (AM1975, Ambion Austin, TX). Briefly, 1 ml of 100% xylene was added to 3 pieces of 20 mm thick FFPE sections. Samples were incubated for 3 min at 50°C to remove traces of paraffin and centrifuged for 2 min to remove the xylene. Pellets were washed twice with 1 ml of 100% ethanol, digested with 200 µl of proteinase K digestive buffer at 50°C overnight and then incubated with DNase I. Samples were washed, total RNA was eluted with distilled water and the RNA concentration of each sample was

determined by a Nanodrop 2000 spectrophotometer. IScript™ cDNA Synthesis Kit was used to generate cDNA and Q-PCR was performed for human *NLRX1* (Hs00226360_m1), *GAPDH* (Hs02758991_g1), *ACTB* (Hs01060665_g1) and *18S rRNA* (Hs03928985_g1). All samples were analyzed in triplicate. Relative mRNA expression levels were determined by the $2^{-\Delta\Delta CT}$ or log-transformed method.

Statistics for Clinical Human Samples: For the analysis of clinical human samples, ratios of real-time PCR values of case-matched normal and CRC tissues were determined. Normalization was performed by determining the mean expression value of three internal control genes: *ACTB*, *GAPDH* and *18S rRNA*. Differences between two sample groups were analyzed using the paired or unpaired Student's t-test (Mann–Whitney unpaired test or Wilcoxon matched-pairs signed test). The association between gene expression levels and clinical parameters was performed by the analysis of variance (ANOVA). A *p* value that is <0.05 is considered statistically significant. All statistical analysis was performed using the Graph pad Prism software.

SUPPLEMENTAL REFERENCES

Allen, I.C., TeKippe, E.M., Woodford, R.M., Uronis, J.M., Holl, E.K., Rogers, A.B., Herfarth, H.H., Jobin, C., and Ting, J.P. (2010). The NLRP3 inflammasome functions as a negative regulator of tumorigenesis during colitis-associated cancer. The Journal of experimental medicine *207*, 1045-1056.

Cancer Genome Atlas, N. (2012). Comprehensive molecular characterization of human colon and rectal cancer. Nature *487*, 330-337.

Ding, S., Blue, R.E., Morgan, D.R., and Lund, P.K. (2014). Comparison of multiple enzyme activatable near-infrared fluorescent molecular probes for detection and quantification of inflammation in murine colitis models. Inflammatory bowel diseases *20*, 363-377.

Ding, S., Eric Blue, R., Chen, Y., Scull, B., Kay Lund, P., and Morgan, D. (2012). Molecular imaging of gastric neoplasia with near-infrared fluorescent activatable probes. Molecular imaging *11*, 507-515.

Fuller, M.K., Faulk, D.M., Sundaram, N., Mahe, M.M., Stout, K.M., von Furstenberg, R.J., Smith, B.J., McNaughton, K.K., Shroyer, N.F., Helmrath, M.A., and Henning, S.J. (2013). Intestinal stem cells remain viable after prolonged tissue storage. Cell Tissue Res *354*, 441-450.

Gaedcke, J., Grade, M., Jung, K., Camps, J., Jo, P., Emons, G., Gehoff, A., Sax, U., Schirmer, M., Becker, H.*, et al.* (2010). Mutated KRAS results in overexpression of DUSP4, a MAP-kinase phosphatase, and SMYD3, a histone methyltransferase, in rectal carcinomas. Genes, chromosomes & cancer *49*, 1024-1034.

Graudens, E., Boulanger, V., Mollard, C., Mariage-Samson, R., Barlet, X., Gremy, G., Couillault, C., Lajemi, M., Piatier-Tonneau, D., Zaborski, P.*, et al.* (2006). Deciphering cellular states of innate tumor drug responses. Genome biology *7*, R19.

Jaffer, F.A., Vinegoni, C., John, M.C., Aikawa, E., Gold, H.K., Finn, A.V., Ntziachristos, V., Libby, P., and Weissleder, R. (2008). Real-time catheter molecular sensing of inflammation in proteolytically active atherosclerosis. Circulation *118*, 1802-1809.

Kaiser, S., Park, Y.K., Franklin, J.L., Halberg, R.B., Yu, M., Jessen, W.J., Freudenberg, J., Chen, X., Haigis, K., Jegga, A.G.*, et al.* (2007). Transcriptional recapitulation and subversion of embryonic colon development by mouse colon tumor models and human colon cancer. Genome biology *8*, R131.

Liu, R., Truax, A.D., Chen, L., Hu, P., Li, Z., Chen, J., Song, C., Chen, L., and Ting, J.P. (2015). Expression profile of innate immune receptors, NLRs and AIM2, in human colorectal cancer: correlation with cancer stages and inflammasome components. Oncotarget *6*, 33456-33469.

Meira, L.B., Bugni, J.M., Green, S.L., Lee, C.-W., Pang, B., Borenshtein, D., Rickman, B.H., Rogers, A.B., Moroski-Erkul, C.A., McFaline, J.L.*, et al.* (2008). DNA damage induced by chronic inflammation contributes to colon carcinogenesis in mice. The Journal of clinical investigation *118*, 2516-2525.

Neufert, C., Becker, C., and Neurath, M.F. (2007). An inducible mouse model of colon carcinogenesis for the analysis of sporadic and inflammation-driven tumor progression. Nature protocols *2*, 1998-2004.

Skrzypczak, M., Goryca, K., Rubel, T., Paziewska, A., Mikula, M., Jarosz, D., Pachlewski, J., Oledzki, J., and Ostrowski, J. (2010). Modeling oncogenic signaling in colon tumors by multidirectional analyses of microarray data directed for maximization of analytical reliability. PLoS One *5*.

Uronis, J.M., Mühlbauer, M., Herfarth, H.H., Rubinas, T.C., Jones, G.S., and Jobin, C. (2009). Modulation of the Intestinal Microbiota Alters Colitis-Associated Colorectal Cancer Susceptibility. PLoS ONE *4*, e6026.

Wang, L., Yao, Z.Q., Moorman, J.P., Xu, Y., and Ning, S. (2014). Gene expression profiling identifies IRF4-associated molecular signatures in hematological malignancies. PLoS One *9*, e106788.

Zhang, H., Morgan, D., Cecil, G., Burkholder, A., Ramocki, N., Scull, B., and Lund, P.K. (2008). Biochromoendoscopy: molecular imaging with capsule endoscopy for detection of adenomas of the GI tract. Gastrointestinal endoscopy *68*, 520-527.